

Theoretical evidence for new adsorption sites of CO₂ on the Ag electrode surface

Shuai Guo,^{a,b} Yao Li,^a Lei Liu,^{a*} Xiangping Zhang,^{a,c} Suojiang Zhang,^{a*}

^a CAS Key Laboratory of Green Process and Engineering, State Key Laboratory of Multiphase Complex Systems, Beijing Key Laboratory of Ionic Liquids Clean Process, Institute of Process Engineering, Chinese Academy of Sciences, Beijing 100190, China

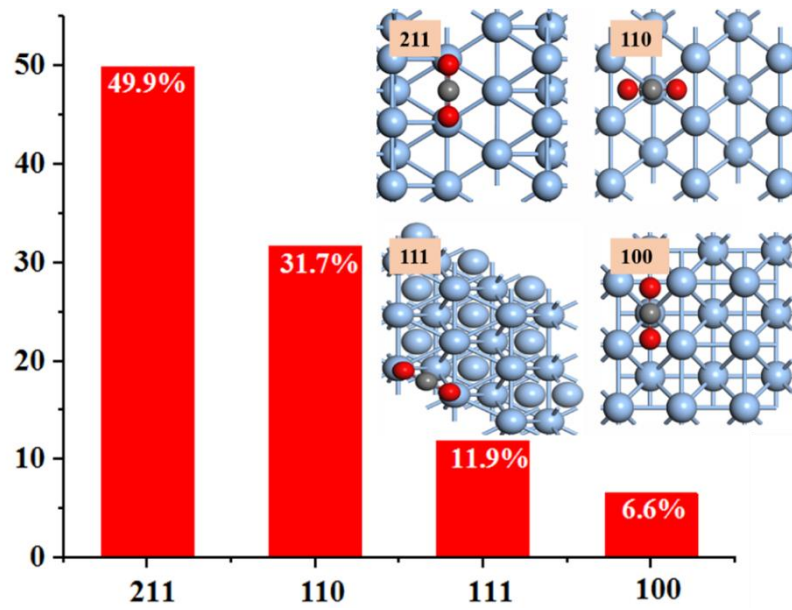
^b School of Future Technology, University of Chinese Academy of Sciences, Beijing 100049, China

^c Dalian National Laboratory for Clean Energy, Dalian 116023, China

ABSTRACT: Nowadays, electrochemical reduction of CO₂ has been considered as an effective method to solve the problem of global warming. The primary challenge in studying the mechanism is to determine the adsorption states of CO₂, since complicated metal surfaces often result in many different adsorption sites. Based on the density functional theory (DFT) calculations, we performed a theoretical study on the adsorption of CO₂ on the Ag electrode surface. The results show that the adsorption populations of CO₂ are extremely sensitive to the adsorption sites. Importantly, we found that the preferable adsorption positions are the terrace sites, rather than the previous reported step sites. The adsorption populations were found with the order of (211) > (110) > (111) > (100). Subsequently, the adsorption characteristics were correlated with the *d*-band theory and the charge transfers between Ag surfaces and CO₂.

KEYWORDS: Electrocatalysis, CO₂ adsorption, Silver, Density functional theory,

TOC: Density functional theory calculations realized that the most stable adsorption positions of CO₂ on Ag surfaces are the terrace sites, rather than the previous reported step sites, and (211) facet is the most populated surface.



INTRODUCTION

Converting the CO₂ into valuable fossil fuels not only resolve the energy shortage, but also alleviates the global warming.¹ Researchers have come up with a variety of methods and techniques to convert CO₂.²⁻⁴ Examples include but not limited to electrochemical, photocatalytic, thermochemical and enzymatic reduction of CO₂. Among them, the electrochemical reduction is one of the most promising methods, which has attracted extensive interests from researchers because of its high product selectivity and mild reaction conditions.⁵⁻⁷ With this technique, CO₂ can be reduced into important products, such as CO, formic acid (HCOOH), ethanol (CH₃CH₂OH) and ethylene (CH₂CH₂), etc.⁸⁻¹⁴ For example, Rosen et al.¹¹ reported the Faraday efficiency (FE) of 96% for CO₂ conversion to CO in the acidic solution (sulfuric acid and 1-ethyl-3-methylimidazoliumtetra-fluoroborate, [Emim][BF₄]) with a silver (Ag) electrode. Hollingsworth et al.¹⁵ reported that the main product was HCOOH (FE>93%) with the same Ag electrode but using a superbase solvent (tetraalkyl phosphonium, [P₆₆₆₁₄][124Triz]). Ma et al.¹⁶ found that the sulfur-doped indium catalyst exhibited a high FE of HCOOH (>85%), a wide current density range (25~100 mA cm⁻²), and a high generation rate of the HCOOH (1449 mol h⁻¹ cm⁻²). Interestingly, Sargent et al. found that by modifying the catalyst surface with organic molecules (aromatic substituted bipyridine), the FE of converting CO₂ to CH₃CH₂OH reach 41%,¹³ which was further enhanced to 43 % if a catalyst of (Ce(OH)_x-doped-Cu) was employed.⁶ With the same methodology, Sargent et al.¹⁴ obtained a FE of CO₂ converting to CH₂CH₂ being 72% (current density 230 mA/cm²).

Meanwhile, the mechanism of electrocatalytic CO₂ reduction reaction (CO₂RR) has been extensively investigated.¹⁷⁻²⁰ On this aspect, understanding CO₂ adsorption behaviors on electrode surfaces is an essential step, which attracts a large number of

studies.²¹⁻²⁵ According to the geometric characteristics and electronic structures of CO₂, its adsorption state generally can be classified into chemical and physical adsorption²⁶⁻²⁸, which is strongly depend on the types of metal electrodes.²⁹⁻³¹ Wang et al. found that CO₂ is physically adsorbed on the Au (111) and Ag (111) surfaces, while it has chemical interactions with Fe, Co, Ni, Cu, Rh, Pd and Pt electrodes (*i.e.* binding energies range from -0.68 to 1.01 eV, and the charge transfer between these metals and the CO₂ is between -0.37 and -0.83 *e*).²⁸ The adsorption of CO₂ on different surfaces of the same electrode can be also different.^{27, 32} For example, Solymosi et al.²⁹ found that CO₂ decomposes on Fe (111) and Fe (100) surfaces. However, there is no decomposition of CO₂ on the Fe (110) surface based on the ultraviolet photoelectron spectroscopy.

For the conversion of CO₂ to CO, Ag is the most often used electrode.^{11, 33-35} Although there have been many experimental³⁶⁻³⁸ and theoretical studies^{28, 39} on the adsorption of CO₂, the preferable adsorption site is still under debate. For example, Zhang et al.³⁹ reported the adsorption energies of CO₂ are -0.01, -0.01, -0.02, and -0.02 eV on (100), (111), (110), and (211) surfaces, respectively. However, Ko et al.²⁰ reported the adsorption energies of CO₂ are -0.26 eV at *bridge*, *hcp* and *fcc* sites on the (111) surface, and the adsorption energies of CO₂ at the equivalent sites on the (111) surface reported by Dietz et al.⁴⁰ were also -0.26 eV. Moreover, similar to other metals (*i.e.* Ru, Pt, Mo), Ag also has multiple adsorption sites on different surfaces.⁴⁰⁻⁴² However, it is still not clear that which is the most stable adsorption site. For this vein, we performed DFT calculations with the goals as follows: 1) to find the most stable adsorption site, and 2) to identify the most populated surface of CO₂. Through this study, we obtained new adsorption sites of CO₂, and the populations of CO₂ on different Ag surfaces. Subsequently, the *d*-band theory, the electronic structures of CO₂ and Ag

surfaces were employed to understand the stabilities of the surfaces and the adsorption behaviors.

COMPUTATIONAL METHODS

The surfaces of (211), (110), (111) and (100) were selected to study the adsorption of CO₂. The experimental lattice constants (4.085 Å) was adopted, which is similar to the previous computational studies.⁴³⁻⁴⁵ Our models contained a 3 × 3 supercell with four Ag layers, of which the bottom two layers were fixed during the optimizations. A vacuum of 15 Å was added above Ag surfaces. The density functional theory calculations were performed by employing the *Vienna ab initio* simulation package (VASP).⁴⁶ The generalized gradient approximation (GGA) Perdew–Burke–Ernzerhof (PBE) functional was used to describe the electronic structure properties of molecules and surfaces.⁴⁷ For ion relaxation, the force convergence was less than 0.05 eV/Å, and the energy convergence was 10⁻⁵ eV. The plane-wave basis cutoff was set to 450 eV. The D3 correction of Grimme was added to all calculations.⁴⁸ The Γ -centered k -point Monkhorst–Pack grid was set to be 1 × 1 × 1 for relaxation, while 12×12×1 k -point was applied for d -band center calculations. The Bader charge was calculated by the code of the Henkelman group.⁴⁹ Factors that may affect the adsorption energies were benchmarked, including system sizes, lattice parameters, k -points, and energy cut-off, which are provided in the Supporting Information.

The adsorption energies of CO₂ (E_{ads}) are calculated by the equation 1:

$$E_{\text{ads}} = E(\text{CO}_2/\text{slab}) - [E(\text{CO}_2) + E(\text{slab})] \quad (1)$$

where $E(\text{CO}_2/\text{slab})$ is the total electronic energy of the Ag surfaces and CO₂, $E(\text{CO}_2)$ is the electronic energy of CO₂, and $E(\text{slab})$ is the electronic energy of the clean Ag surface.

According to Boltzmann distributions, the population of CO₂ at each adsorption site are calculated *via* equation 2.⁵⁰

$$P_i = \frac{e^{-\varepsilon_i/kT}}{\sum_{j=1}^M e^{-\varepsilon_j/kT}} \quad (2)$$

where P_i is the probability of particle distribution at position i , ε_i is the adsorption energy at position i , k is the Boltzmann constant, and T is the temperature (298.15 K).

RESULTS AND DISCUSSION

The adsorption sites of CO₂ on Ag surfaces are listed in Fig. 1(a) ~ (d). Specifically, fourteen adsorption sites are found on the (211) surface, including three *top* sites (T1, T2, and T3), six *bridge* sites (B1, B2, B3, B4, B5, and B6), and five *hollow* sites (H1, H2, H3, H4, and H5). The (110) surface has seven adsorption sites, including two *top* sites (T1 and T2), three *bridge* sites (B1, B2, and B3) and two *hollow* sites (H1 and H2). The (111) surface has four adsorption sites, which are one *top* (T), one *bridge* (B), one *two-fold hollow* (H) and one *three-fold hollow* (F), respectively. There are three adsorption sites on the surface of (100), which are one *top* (T), one *bridge* (B), and one *two-fold hollow* (H). On the other hand, CO₂ has four, four, seven and three possible orientations on (211), (110), (111) and (100) surfaces, respectively (see Fig. 2, and Fig. S1~ S3). In total, we found 56, 28, 13 and 9 structures of CO₂ adsorbed on (211), (110), (111) and (100) surfaces, respectively. For clarify, we employed labels for each structure with a rule as follows: preceding letters (including numbers) represent adsorption sites of CO₂, and the last letter (*a*, *b*, *c*, and *d*) represent the orientation of CO₂. For example, T1a refers to the T1 site (Fig.1) with *a* orientation of CO₂ (Fig.2).

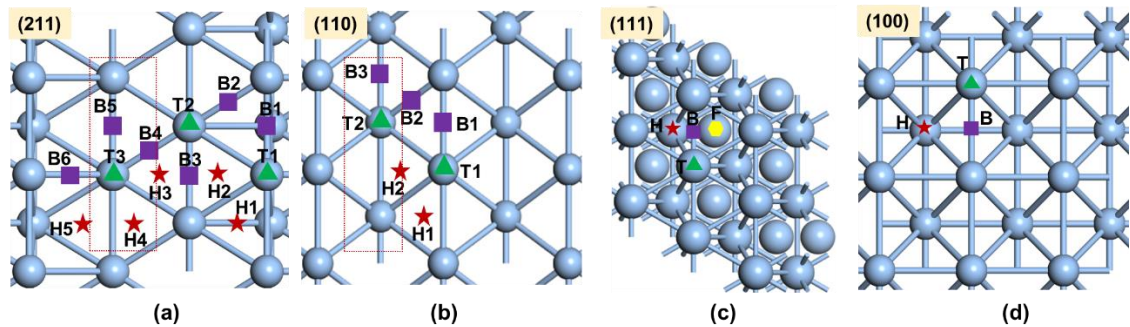


Figure. 1. Top views of (a) (211), (b) (110), (c) (111), (d) (100) surfaces. The red dashed line in (a) and (b) are for the convenience of later discussion.

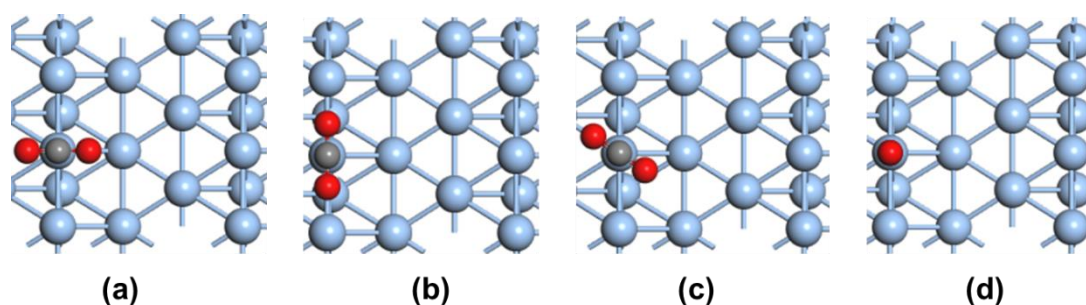


Figure. 2. Top views of CO₂ orientations at the T1 site of the (211) surface, and top view of CO₂ orientations on other surfaces are shown in Fig. S1~S3. Color legend: Ag grey, C black and O red.

According to previous studies,³⁹ initial distances between CO₂ and the (211) surface were set as 3.3 Å, and CO₂ were set to be linear ($\angle\text{OCO}=180^\circ$). The selected optimized structures and corresponding adsorption energies are shown in Fig. 3 (for all structures and their adsorption energies, see Fig. S4 and Table S1). Of these structures, B5b and H4c have the largest adsorption energies (*i.e.*, -0.29 eV). The distances between CO₂ and nearest Ag atom are $d_{\text{C-Ag}} = 3.7$ Å, $d_{\text{O1-Ag}} = 3.6$ Å, $d_{\text{O2-Ag}} = 3.6$ Å for B5b, and $d_{\text{C-Ag}} = 3.6$ Å, $d_{\text{O1-Ag}} = 3.5$ Å, $d_{\text{O2-Ag}} = 3.6$ Å for H4c, respectively. The next two meta-stable structures are T3a and B4c, and their adsorption energies are -0.28 eV. The distances from O and C to the nearest Ag are $d_{\text{C-Ag}} = 3.9$ Å, $d_{\text{O1-Ag}} = 3.6$ Å, $d_{\text{O2-Ag}} = 3.9$ Å for T3a, and $d_{\text{C-Ag}} = 3.6$ Å, $d_{\text{O1-Ag}} = 3.4$ Å, $d_{\text{O2-Ag}} = 3.7$ Å for B4c, respectively. Note that Zhang et al.³⁹ reported the adsorption energy of CO₂ is -0.02 eV when Van der Waals (vdW) corrections are not included in the DFT calculations. We also computed the adsorption energies of CO₂ at T1, T2, T3 and B1 without vdW corrections, which are -0.02, -0.03, -0.02 and -0.02 eV, respectively (Table S3). Besides the geometric characteristics of the CO₂, Bader charge analysis also confirm that CO₂ is physically adsorbed on the (211) surface. For example, the charge transfers between

CO₂ and the (211) surface are only 0.061 *e* for B5b, 0.050 *e* for T2a, and 0.041 *e* for T1b, respectively. Notably, we found that the adsorption energies of CO₂ vary largely with respect to the adsorption sites. Generally, the terrace sites (B5, B4, H4 and T3, highlighted with the red dot box in Fig.1a) have larger values than that of the step (*i.e.* B1, B6, H1 and T1). For example, the adsorption energy of B5b is -0.29 eV, while the adsorption energy of T1b is -0.15 eV (Fig. 3).

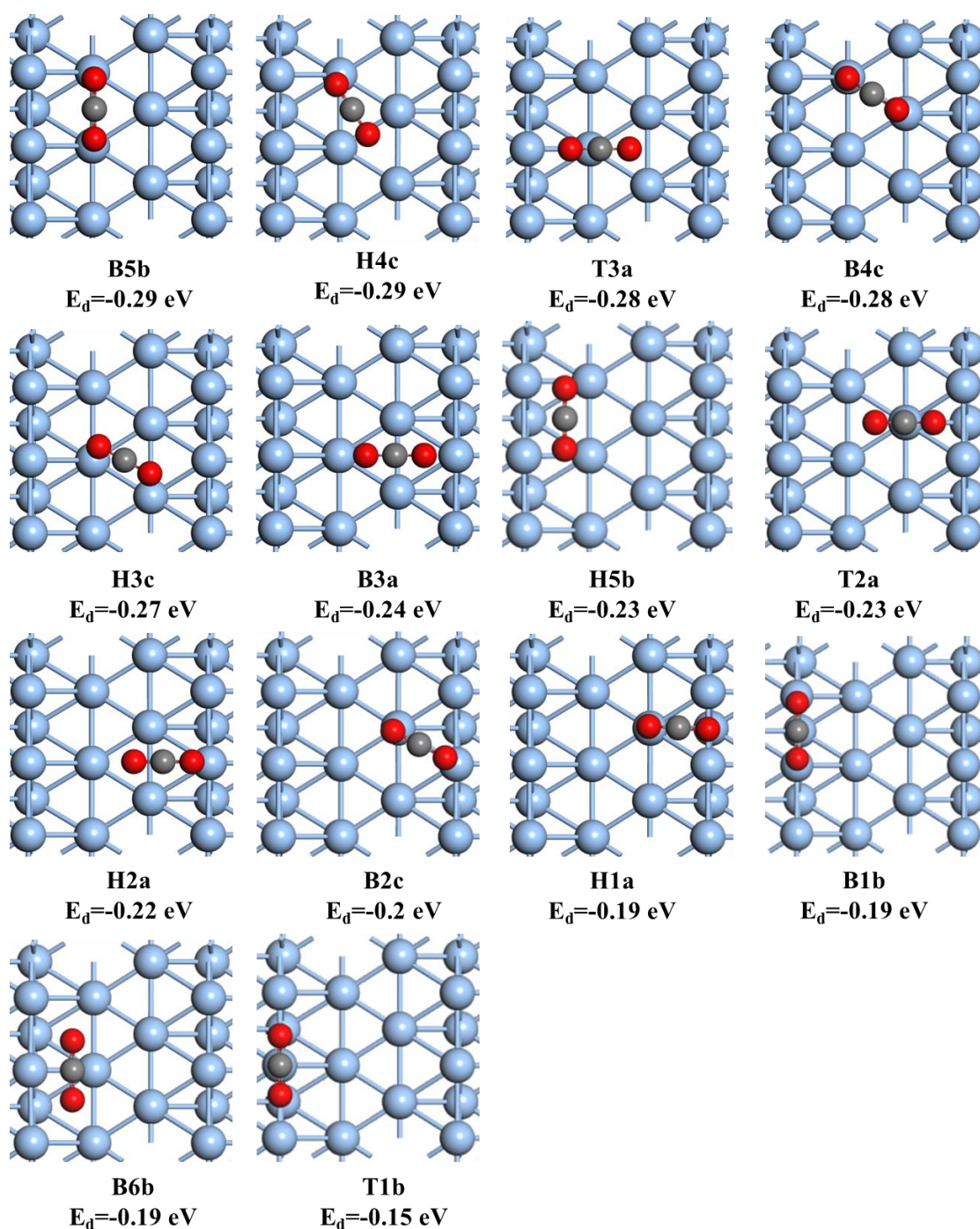


Figure. 3. Top views of optimized structures of the (211) surface, which are sorted by the adsorption energies. Color legend: Ag grey, C black and O red.

Based on the DFT calculations, Wang et al.²⁷ found that the adsorption energies are somehow dependent on the coverage of CO₂. Here, we selected four representative sites (*i.e.*, T1, T2, T3, and B1 of the (211) surface), and changed the coverage from 1/9 to 1/18. As shown in Table S4, adsorption energy differences are negligible, which are less than 0.02 eV. Importantly, the order of the adsorption energies remained the same. Moreover, we additionally considered structural models with the CO₂ having chemical interactions with the surface (distances between CO₂ and the (211) surface are set as 2.2 Å, and ∠OCO as 120° and 180°, see Fig. S5). The DFT calculations show that the structures and the adsorption energies are almost the same to that depicted in Fig. 3 and Fig. S4 (see Table S5).

The selected optimized structures and corresponding adsorption energies of CO₂ on the second commonly studied (110) surface are shown in Fig. 4, and the full list of the optimized structures are given in Fig. S6, with the corresponding adsorption energies listed in Table S6. Similar to that of the (211) surface, the adsorption energies are strongly dependent on the adsorption sites. Generally, the adsorption energies at T2, B3, H2 and B2 sites are relatively larger, and these adsorption positions are either at or close to the terrace sites, which are marked with the red dotted box in Fig. 1b. The positions lie on the step sites have relatively smaller adsorption energies (*i.e.* H1, B1 and T1). In the stable structures (*i.e.* T2a, B3a, and H2a in Fig. 4), the distances between C and the nearest Ag are 3.7 Å, 3.5 Å, 3.4 Å, respectively, and distances from O to the nearest Ag are 3.2 Å (3.3 Å), 2.9 Å, 3.0 Å (3.2 Å), respectively. The values of d_{O-Ag} and d_{C-Ag} of all structures are listed in Table S7. Moreover, the Bader charge analysis shows charge transfers between CO₂ and the (110) surface are 0.058 e for T2a, 0.053 e

for B2a, and 0.046 e for B1b. Based on these calculations, we conclude that the adsorption of CO₂ on the (110) surface are again the physical adsorption, which is the same to that of the (211) surface. Moreover, previous studies^{36,51} also reported the weak interactions of CO₂ with the (110) surface by the electron energy loss spectroscopy (EELS), low energy electron diffraction (LEED) and temperature programmed desorption (TPD).

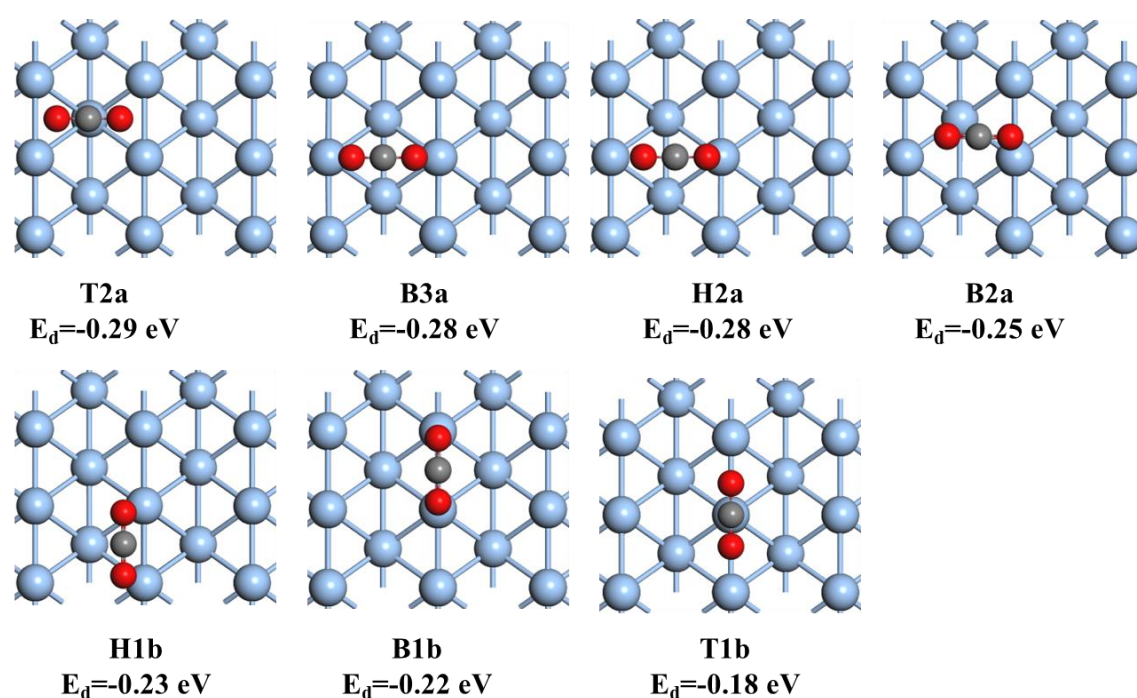


Figure 4. Top view of optimized structures of the (110) surface, which are sorted by the adsorption energies. Color legend: Ag grey, C black and O red.

For the CO₂ on the (111) surface, we optimized thirteen adsorption structures (see Fig. S7). The most stable structures and corresponding adsorption energies are shown in Fig. 5. DFT calculations show that adsorption energies at B, H and F sites are similar (-0.26 eV), which are higher than that at the T site (-0.23 eV). The largest adsorption energy at B, H and F sites on the (111) surface is -0.26 eV, and the Bader charge analysis shows charge transfers between CO₂ and (111) surface is 0.055 e for Fa and Ha, and 0.051 e for Ta, respectively. These calculations indicate that the adsorption of

CO₂ on the (111) surface belongs to the physical adsorption, which is similar to the previous experimental results obtained by the low energy electron diffraction (LEED).⁵² Moreover, nine structures were considered for the CO₂ on the (100) surface (Fig. S8), and the most stable adsorption structures and corresponding adsorption energies are shown in Fig. 5. We found that the order of adsorption energies at follow an order of H>B>T, and the most stable structure on the (100) surface is Ha, having an adsorption energy of -0.26 eV. The Bader charge analysis also confirmed the physical adsorption characteristics of the CO₂ on the (100) surface. For example, the corresponding distances of O and C to the nearest Ag for the Ha structure ($d_{C-Ag} = 3.6 \text{ \AA}$, $d_{O1-Ag} = 3.3 \text{ \AA}$, $d_{O2-Ag} = 3.3 \text{ \AA}$). The Bader charge analysis shows charge transfers between CO₂ and the (100) surface are 0.049 *e* for Ha, 0.043 *e* for Ba, and 0.037 *e* for Ta, respectively.

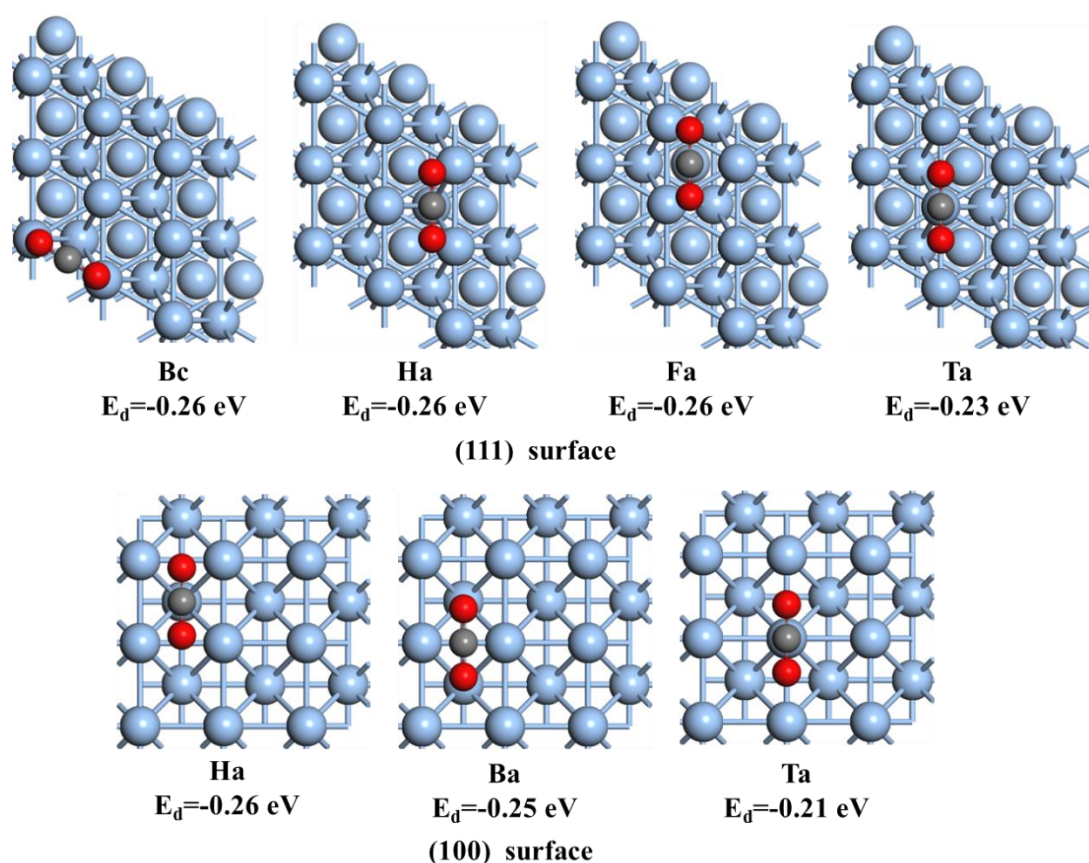


Figure 5. Top view of the optimized structures of (111) and (100) surfaces, which are sorted by the adsorption energies. Color legend: Ag grey, C black and O red.

Lastly, based on the adsorption energies, we calculated the populations of CO₂ on different Ag surfaces by employing Boltzmann distributions (Eq. 2), and the results are given in Table 1. The results show that the populations of CO₂ on four surfaces are different, having the order of (211) > (110) > (111) > (100). The possibilities of locating CO₂ on (211) and (110) surfaces are 49.85%, and 31.7%, respectively. The summation of 81.55% indicates that these two surfaces are the most reactive facets to capture the CO₂. However, the other two surfaces, (111) and (100) only have possibilities of 11.91% and 6.55%, respectively to capture the CO₂. Moreover, the populations of CO₂ on different adsorption sites are also different even for the same surface. Taking the (211) surface as an example, CO₂ at B5 and T1 sites are 11.56 % and 0.05%, respectively. Interestingly, we found that populations of CO₂ at step sites (T or T1) are the lowest for all surfaces, which is contrary to the common belief where the populations at T (or T1) are the highest.³⁹ In contrast, the populations of CO₂ at the terrace sites are the highest for all studied surfaces. For example, the B5 at the (211) and T2 at the (110) surface. To further verify the rules presented in Table 1, we calculated the *d*-band center of (211), (110), (111) and (100) surfaces, which are -3.70 eV, -3.97 eV, -4.02 eV, -4.14 eV, respectively, which are similar to the reported values of -4.04 eV for the *d*-band center of (111).⁵³ The results of the linearly correlation between the adsorption possibilities and the positions of *d*-band center support our findings on the population of CO₂ on Ag surfaces.^{35,68} Moreover, we calculated charge transfers between CO₂ and Ag surfaces, and we found that increasing charge transfer between CO₂ and Ag surfaces makes the structures more stable when CO₂ is adsorbed on the metal surfaces.⁵²

Table 1. The populations of CO₂ at the adsorption sites of (211), (110), (111) and (100) surfaces. The corresponding optimized structures and adsorption energies are provided in Fig.3 ~Fig.5.

(211)		(110)		(111)		(100)			
sites	%	sites	%	sites	%	sites	%	sites	%
B5	11.56	T2	1.12	T2	11.56	B	3.60	H	3.60
H4	11.56	H2	0.76	B3	7.83	H	3.60	B	2.44
T3	7.83	B2	0.35	H2	7.83	F	3.60	T	0.51
B4	7.83	H1	0.24	B2	2.44	T	1.12	--	--
H3	5.31	B1	0.24	H1	1.12	--	--	--	--
B3	1.65	B6	0.24	B1	0.76	--	--	--	--
H5	1.12	T1	0.05	T1	0.16	--	--	--	--
Sum			49.85		31.70		11.91		6.55

CONCLUSIONS

As a summary, the adsorption states of CO₂ on (211), (110), (111), and (100) surfaces of the Ag electrode were investigated by DFT calculations. The most stable CO₂ adsorption sites are found for all studies as well as their adsorption structures. Adsorption populations of CO₂ on different surfaces are found with the order of (211) > (110) > (111) > (100). The most stable adsorption positions are not the previous reported step sites, but the terrace sites. CO₂ is mainly adsorbed by vdW interactions, and there is very little charge transfer (< 0.1 *e*) between CO₂ and Ag surfaces. The adsorption energies of CO₂ vary largely at different adsorption sites on the same Ag surface, which is somehow corrected with *d*-band center positions and the charge transfers between Ag surfaces and CO₂.

ASSOCIATED CONTENT

Supporting Information

The Supporting Information is available free of charge on the ACS Publications website.

The benchmarked calculations, adsorption energies, and optimized structures.

AUTHOR INFORMATION

Corresponding authors:

Lei Liu, liulei@ipe.ac.cn; liulei3039@gmail.com

Suojiang Zhang, sjzhang@ipe.ac.cn

Notes

The authors declare no competing financial interest.

ACKNOWLEDGMENTS

This work was financially supported by the Key Program of National Natural Science Foundation of China (21978306), DNL Cooperation Fund, CAS (DNL180406) and the CAS Pioneer Hundred Talents Program (L. L).

REFERENCES

1. Benson, E. E.; Kubiak, C. P.; Sathrum, A. J.; Smieja, J. M. Electrocatalytic and homogeneous approaches to conversion of CO₂ to liquid fuels. *Chem. Soc. Rev.* **2009**, *38* (1), 89-99.
2. Kondratenko, E. V.; Mul, G.; Baltrusaitis, J.; Larrazábal, G. O.; Pérez-Ramírez, J. Status and perspectives of CO₂ conversion into fuels and chemicals by catalytic, photocatalytic and electrocatalytic processes. *Energy Environ. Sci.* **2013**, *6* (11), 3112-3135.
3. Takeda, H.; Kamiyama, H.; Okamoto, K.; Irimajiri, M.; Mizutani, T.; Koike, K.; Sekine, A.; Ishitani, O. Highly Efficient and Robust Photocatalytic Systems for CO₂ Reduction Consisting of a Cu(I) Photosensitizer and Mn(I) Catalysts. *J. Am. Chem. Soc.* **2018**, *140* (49), 17241-17254.
4. Seh, Z. W.; Kibsgaard, J.; Dickens, C. F.; Chorkendorff, I.; Nørskov, J. K.; Jaramillo, T. F. Combining theory and experiment in electrocatalysis: Insights into materials design. *Science* **2017**, *355* (6321), eaad4998.

5. Li, C. W.; Ciston, J.; Kanan, M. W. Electroreduction of carbon monoxide to liquid fuel on oxide-derived nanocrystalline copper. *Nature* **2014**, *508* (7497), 504-507.
6. Luo, M.; Wang, Z.; Li, Y. C.; Li, J.; Li, F.; Lum, Y.; Nam, D.-H.; Chen, B.; Wicks, J.; Xu, A.; Zhuang, T.; Leow, W. R.; Wang, X.; Dinh, C.-T.; Wang, Y.; Wang, Y.; Sinton, D.; Sargent, E. H. Hydroxide promotes carbon dioxide electroreduction to ethanol on copper via tuning of adsorbed hydrogen. *Nat. Commun.* **2019**, *10* (1), 5814.
7. Li, J.; Wang, Z.; McCallum, C.; Xu, Y.; Li, F.; Wang, Y.; Gabardo, C. M.; Dinh, C.-T.; Zhuang, T.-T.; Wang, L.; Howe, J. Y.; Ren, Y.; Sargent, E. H.; Sinton, D. Constraining CO coverage on copper promotes high-efficiency ethylene electroproduction. *Nat. Catal* **2019**, *2* (12), 1124-1131.
8. Kattel, S.; Ramírez, P. J.; Chen, J. G.; Rodriguez, J. A.; Liu, P. Active sites for CO₂ hydrogenation to methanol on Cu/ZnO catalysts. *Science* **2017**, *355* (6331), 1296-1299.
9. Cheng, T.; Xiao, H.; Goddard, W. A. Free-Energy Barriers and Reaction Mechanisms for the Electrochemical Reduction of CO on the Cu(100) Surface, Including Multiple Layers of Explicit Solvent at pH 0. *J. Phys. Chem. Lett.* **2015**, *6* (23), 4767-4773.
10. Gao, S.; Lin, Y.; Jiao, X.; Sun, Y.; Luo, Q.; Zhang, W.; Li, D.; Yang, J.; Xie, Y. Partially oxidized atomic cobalt layers for carbon dioxide electroreduction to liquid fuel. *Nature* **2016**, *529* (7584), 68-71.
11. Rosen, B. A.; Salehi-Khojin, A.; Thorson, M. R.; Zhu, W.; Whipple, D. T.; Kenis, P. J. A.; Masel, R. I. Ionic Liquid-Mediated Selective Conversion of CO₂ to CO at Low Overpotentials. *Science* **2011**, *334* (6056), 643-644.
12. Cheng, T.; Xiao, H.; Goddard, W. A. Reaction Mechanisms for the Electrochemical Reduction of CO₂ to CO and Formate on the Cu(100) Surface at 298 K from Quantum Mechanics Free Energy Calculations with Explicit Water. *J. Am. Chem. Soc.* **2016**, *138* (42), 13802-13805.
13. Li, F.; Li, Y. C.; Wang, Z.; Li, J.; Nam, D.-H.; Lum, Y.; Luo, M.; Wang, X.; Ozden, A.; Hung, S.-F.; Chen, B.; Wang, Y.; Wicks, J.; Xu, Y.; Li, Y.; Gabardo, C. M.; Dinh, C.-T.; Wang, Y.; Zhuang, T.-T.; Sinton, D.; Sargent, E. H. Cooperative CO₂-to-ethanol conversion via enriched intermediates at molecule-metal catalyst interfaces. *Nat. Catal* **2020**, *3* (1), 75-82.
14. Li, F.; Thevenon, A.; Rosas-Hernández, A.; Wang, Z.; Li, Y.; Gabardo, C. M.; Ozden, A.; Dinh, C. T.; Li, J.; Wang, Y.; Edwards, J. P.; Xu, Y.; McCallum, C.; Tao, L.; Liang, Z.-Q.; Luo, M.; Wang, X.; Li, H.; O'Brien, C. P.; Tan, C.-S.; Nam, D.-H.; Quintero-Bermudez, R.; Zhuang, T.-T.; Li, Y. C.; Han, Z.; Britt, R. D.; Sinton, D.; Agapie, T.; Peters, J. C.; Sargent, E. H. Molecular tuning of CO₂-to-ethylene conversion. *Nature* **2020**, *577* (7791), 509-513.
15. Hollingsworth, N.; Taylor, S. F. R.; Galante, M. T.; Jacquemin, J.; Longo, C.; Holt, K. B.; de Leeuw, N. H.; Hardacre, C. Reduction of Carbon Dioxide to Formate at Low Overpotential Using a Superbase Ionic Liquid. *Angew. Chem. Int. Ed.* **2015**, *54* (47), 14164-14168.
16. Burdyny, T.; Smith, W. A. CO₂ reduction on gas-diffusion electrodes and why catalytic performance must be assessed at commercially-relevant conditions. *Energy Environ. Sci.* **2019**, *12* (5), 1442-1453.
17. Grabow, L. C.; Mavrikakis, M. Mechanism of Methanol Synthesis on Cu through CO₂ and CO Hydrogenation. *ACS Catal.* **2011**, *1* (4), 365-384.

18. Muttaqien, F.; Hamamoto, Y.; Inagaki, K.; Morikawa, Y. Dissociative adsorption of CO₂ on flat, stepped, and kinked Cu surfaces. *J. Chem. Phys.* **2014**, *141* (3), 034702.
19. Wang, W.; Wang, S.; Ma, X.; Gong, J. Recent advances in catalytic hydrogenation of carbon dioxide. *Chem. Soc. Rev.* **2011**, *40* (7), 3703-3727.
20. Ko, J.; Kim, B.-K.; Han, J. W. Density Functional Theory Study for Catalytic Activation and Dissociation of CO₂ on Bimetallic Alloy Surfaces. *J. Phys. Chem. C* **2016**, *120* (6), 3438-3447.
21. Liu, W.; Tkatchenko, A.; Scheffler, M. Modeling Adsorption and Reactions of Organic Molecules at Metal Surfaces. *Acc. Chem. Res.* **2014**, *47* (11), 3369-3377.
22. Lynch, M.; Hu, P. A density functional theory study of CO and atomic oxygen chemisorption on Pt(111). *Surf. Sci.* **2000**, *458* (1), 1-14.
23. Jiang, T.; Mowbray, D. J.; Dobrin, S.; Falsig, H.; Hvolbæk, B.; Bligaard, T.; Nørskov, J. K. Trends in CO Oxidation Rates for Metal Nanoparticles and Close-Packed, Stepped, and Kinked Surfaces. *J. Phys. Chem. C* **2009**, *113* (24), 10548-10553.
24. Zhu, B.; Meng, J.; Gao, Y. Equilibrium Shape of Metal Nanoparticles under Reactive Gas Conditions. *J. Phys. Chem. C* **2017**, *121* (10), 5629-5634.
25. Zinola, C. F.; Gomis-Bas, C.; Estiú, G. L.; Castro, E. A.; Arvia, A. J. A Semiempirical Quantum Approach to the Formation of Carbon Dioxide Adsorbates on Pt(100) and Pt(111) Cluster Surfaces. *Langmuir* **1998**, *14* (14), 3901-3908.
26. Freund, H. J.; Messmer, R. P. On the bonding and reactivity of CO₂ on metal surfaces. *Surf. Sci.* **1986**, *172* (1), 1-30.
27. Wang, S.-G.; Cao, D.-B.; Li, Y.-W.; Wang, J.; Jiao, H. Chemisorption of CO₂ on Nickel Surfaces. *J. Phys. Chem. B.* **2005**, *109* (40), 18956-18963.
28. Wang, S.-G.; Liao, X.-Y.; Cao, D.-B.; Huo, C.-F.; Li, Y.-W.; Wang, J.; Jiao, H. Factors Controlling the Interaction of CO₂ with Transition Metal Surfaces. *J. Phys. Chem. C* **2007**, *111* (45), 16934-16940.
29. Solymosi, F. The bonding, structure and reactions of CO₂ adsorbed on clean and promoted metal surfaces. *Journal of Molecular Catalysis* **1991**, *65* (3), 337-358.
30. Rodríguez, C. R. B.; Santana, J. A. Adsorption and diffusion of sulfur on the (111), (100), (110), and (211) surfaces of FCC metals: Density functional theory calculations. *J. Chem. Phys.* **2018**, *149* (20), 204701.
31. Jiang, B.; Guo, H. Communication: Enhanced dissociative chemisorption of CO₂ via vibrational excitation. *J. Chem. Phys.* **2016**, *144* (9), 091101.
32. Wang, G.; Jiang, L.; Morikawa, Y.; Nakamura, J.; Cai, Z.; Pan, Y.; Zhao, X. Cluster and periodic DFT calculations of adsorption and activation of CO₂ on the Cu(hkl) surfaces. *Surf. Sci.* **2004**, *570*, 205-217.
33. Seifitokaldani, A.; Gabardo, C. M.; Burdyny, T.; Dinh, C.-T.; Edwards, J. P.; Kibria, M. G.; Bushuyev, O. S.; Kelley, S. O.; Sinton, D.; Sargent, E. H. Hydronium-Induced Switching between CO₂ Electroreduction Pathways. *J. Am. Chem. Soc.* **2018**, *140* (11), 3833-3837.
34. Asadi, M.; Kim, K.; Liu, C.; Addepalli, A. V.; Abbasi, P.; Yasaei, P.; Phillips, P.; Behranginia, A.; Cerrato, J. M.; Haasch, R.; Zapol, P.; Kumar, B.; Klie, R. F.; Abiade, J.; Curtiss, L. A.; Salehi-Khojin, A. Nanostructured transition metal dichalcogenide electrocatalysts for CO₂ reduction in ionic liquid. *Science* **2016**, *353* (6298), 467.
35. Hatsukade, T.; Kuhl, K. P.; Cave, E. R.; Abram, D. N.; Jaramillo, T. F. Insights into the electrocatalytic reduction of CO₂ on metallic silver surfaces. *Phys. Chem. Chem. Phys.* **2014**, *16* (27), 13814-13819.

36. Backx, C.; De Groot, C. P. M.; Biloen, P.; Sachtler, W. M. H. Interaction of O₂, CO₂, CO, C₂H₄ and C₂H₄O with Ag(110). *Surf. Sci.* **1983**, *128* (1), 81-103.
37. Maynard, K. J.; Moskovits, M. A surface enhanced Raman study of carbon dioxide coadsorption with oxygen and alkali metals on silver surfaces. *J. Chem. Phys.* **1989**, *90* (11), 6668-6679.
38. Backx, C.; de Groot, C. P. M.; Biloen, P. Electron energy loss spectroscopy and its applications. *Appl. Surf. Sci.* **1980**, *6* (3), 256-272.
39. Zhang, X.-G.; Jin, X.; Wu, D.-Y.; Tian, Z.-Q. Selective Electrocatalytic Mechanism of CO₂ Reduction Reaction to CO on Silver Electrodes: A Unique Reaction Intermediate. *J. Phys. Chem. C* **2018**, *122* (44), 25447-25455.
40. Dietz, L.; Piccinin, S.; Maestri, M. Mechanistic Insights into CO₂ Activation via Reverse Water–Gas Shift on Metal Surfaces. *J. Phys. Chem. C* **2015**, *119* (9), 4959-4966.
41. Wang, T.; Tian, X.; Yang, Y.; Li, Y.; Wang, J.; Beller, M.; Jiao, H. Structures of seven molybdenum surfaces and their coverage dependent hydrogen adsorption. *Phys. Chem. Chem. Phys.* **2016**, *18* (8), 6005-6012.
42. Yang, Z.; Zhang, Y.; Guo, M.; Yun, J. Adsorption of hydrogen and oxygen on graphdiyne and its BN analog sheets: A density functional theory study. *Comp. Mater. Sci.* **2019**, *160*, 197-206.
43. Singh, M. R.; Goodpaster, J. D.; Weber, A. Z.; Head-Gordon, M.; Bell, A. T. Mechanistic insights into electrochemical reduction of CO₂ over Ag using density functional theory and transport models. *Proc. Natl. Acad. Sci.* **2017**, *114* (42), E8812-E8821.
44. Back, S.; Yeom, M. S.; Jung, Y. Active Sites of Au and Ag Nanoparticle Catalysts for CO₂ Electroreduction to CO. *ACS Catal.* **2015**, *5* (9), 5089-5096.
45. Solid State Physics. Von N. W. Ashcroft und N. D. Mermin; Holt, Rinehart and Winston, New York 1976, XXII, 826 Seiten, \$19,95. *Physik in unserer Zeit* **1978**, *9* (1), 33-33.
46. Kresse, G.; Furthmüller, J. Efficient iterative schemes for ab initio total-energy calculations using a plane-wave basis set. *Phys. Rev. B* **1996**, *54* (16), 11169-11186.
47. Perdew, J. P.; Burke, K.; Ernzerhof, M. Generalized Gradient Approximation Made Simple. *Phys. Rev. Lett.* **1996**, *77* (18), 3865-3868.
48. Grimme, S.; Ehrlich, S.; Goerigk, L. Effect of the damping function in dispersion corrected density functional theory. *J. Comput. Chem.* **2011**, *32* (7), 1456-1465.
49. Tang, W.; Sanville, E.; Henkelman, G. A grid-based Bader analysis algorithm without lattice bias. *J. Phys.: Condens. Matter* **2009**, *21* (8), 084204.
50. Metropolis, N.; Rosenbluth, A. W.; Rosenbluth, M. N.; Teller, A. H.; Teller, E. Equation of State Calculations by Fast Computing Machines. *J. Chem. Phys.* **1953**, *21* (6), 1087-1092.
51. Bowker, M.; Barteau, M. A.; Madix, R. J. Oxygen induced adsorption and reaction of H₂, H₂O, CO and CO₂ on single crystal Ag(110). *Surf. Sci.* **1980**, *92* (2), 528-548.
52. Sakurai, M.; Okano, T.; Tuzi, Y. Vibrational excitation of physisorbed CO₂ on a Ag(111) surface. *J VAC SCI TECHNOL A* **1987**, *5* (4), 431-434.
53. Vojvodic, A.; Nørskov, J. K.; Abild-Pedersen, F. Electronic Structure Effects in Transition Metal Surface Chemistry. *Top. Catal.* **2014**, *57* (1), 25-32.